Direct Measurement of Energy Transfer in Strongly Driven Rotating Turbulence

Omri Shaltiel, Alon Salhov, Omri Gat, and Eran Sharon
Racah Institute of Physics, The Hebrew University, Jerusalem 91904, Israel

(Received 19 February 2023; accepted 12 April 2024; published 29 May 2024)

A short, abrupt increase in energy injection rate into steady strongly driven rotating turbulent flow is used as a probe for energy transfer in the system. The injected excessive energy is localized in time and space and its spectra differ from those of the steady turbulent flow. This allows measuring energy transfer rates, in three different domains: In real space, the injected energy propagates within the turbulent field, as a wave packet of inertial waves. In the frequency domain, energy is transferred nonlocally to the low, quasigeostrophic modes. In wave number space, energy locally cascades toward small wave numbers, in a rate that is consistent with two-dimensional (2D) turbulence models. Surprisingly however, the inverse cascade of energy is mediated by inertial waves that propagate within the flow with small, but nonvanishing frequency. Our observations differ from measurements and theoretical predictions of weakly driven turbulence. Yet, they show that in strongly driven rotating turbulence, inertial waves play an important role in energy transfer, even in the vicinity of the 2D manifold.

DOI: 10.1103/PhysRevLett.132.224001

Introduction.—Understanding the dynamics governing rotating turbulent flows is important in scientific fields such as geophysics, astrophysics, and atmospheric sciences [1–3]. However, certain fundamental processes governing these flows remain unclear [4]. In particular, the relation between two competing views, that of quasi-two-dimensional (2D) turbulence and that of inertial-wave turbulence, is not clear [5,6].

Rotating incompressible fluids are described by the rotating-frame Navier-Stokes equations (RNSE) and the incompressibility condition. In this work, we consider a system rotating at a constant rate Ω around a vertical axis: $\boldsymbol{\Omega} = \Omega\hat{\boldsymbol{z}}$ ($\hat{}$ marks a unit vector). The system's vertical extent is comparable to its extent in the x, y "horizontal" directions, perpendicular to the axis of rotation. Two dimensionless numbers characterize such systems, the Reynolds number, $\mathrm{Re} = UL/\nu$ and Rossby number, $\mathrm{Ro} = U/(2\Omega L)$, where U and L are the typical velocity and length scales, and ν is the kinematic viscosity. Rotating turbulence emerges when $\mathrm{Re} \gg 1$, indicating the dominance of nonlinear inertial effects over viscous effects, and $\mathrm{Ro} \ll 1$, signifying the dominance of Coriolis acceleration over nonlinear inertial accelerations.

The inviscid linearized RNSE, obtained by dropping the inertial and viscous terms, has solutions of the form of plane inertial-waves [7] with frequency ω and a wave-vector $\boldsymbol{k}$ that obey the dispersion relation [8]:

$$\omega = \pm 2\Omega\cos(\theta), \qquad \cos(\theta) = \hat{\boldsymbol{k}}\cdot\hat{\boldsymbol{z}}, \tag{1}$$

i.e., the frequency does not depend on the magnitude of the wave vector, $k = |\boldsymbol{k}|$, but only on the angle, θ, between $\hat{k}$ and the rotation axis ($\hat{z}$). The vertical component of the group velocity is given by

$$C_{g,z}(\boldsymbol{k}) = \frac{2\Omega\sin^2\theta}{k}. \tag{2}$$

Thus, for a given k, wave packets centered around horizontal wave vectors with $\theta \approx \pi/2$ transfer energy vertically with the highest speed.

Inertial waves, have been observed in experiments [9–13] and simulations [13–15] of rotating turbulence decay and build-up [15–20]. Theoretical descriptions of rotating turbulence that take into account interactions have been derived [14,21–23]; they are typically limited to weak wave turbulence. Indeed, for weakly forced steady turbulence or when the geostrophic flow is suppressed, 3D inertial waves dominate the energy spectrum and energy transfer is mediated by three-wave resonant interactions. Such a behavior was predicted theoretically [21] and first shown in recent experimental work [10,24]. It is also observed in our system, when driven weakly (see Supplemental Material [25], Fig. S2). Yet, at stronger driving, which is relevant to this work, the mode of energy transfer was changed, leading to dominance of the quasigeostrophic flow.

Previous observations indicate that as the rate of rotation increases, the flow field becomes increasingly two-dimensional [4]. Under these conditions, some characteristics of the horizontal flow resemble those of 2D (nonrotating) turbulence [23,26–31], including the inverse cascade of energy from small to large scales. These characteristics, along with vertical uniformity of the flow, persist even when energy is injected locally in space [29], implying the existence of a mechanism homogenizing

energy vertically. Motivated by these observations, models that focus on the energy transfer to the geostrophic component of the flow (flow parallel to the 2D horizontal plane) were derived [14,23,32–36]. However, the precise mechanism underlying this homogenization process remains not fully understood.

These diverse results show that rotating turbulence is spectrally heterogeneous, energetically dominated by the geostrophic quasi-2D flow component, that coexists with the inertial-wave-dominated 3D flow [11,12,33,37–39]. Still, the relationship between these components is not well understood. Specifically, the process by which energy is transferred from 3D to quasi-2D modes, and the role that inertial waves play in the strongly driven turbulence regime, are currently not clear. Because of the flow's three-dimensionality and anisotropy answers to these questions are associated with rates of energy transfer in real space, in the frequency domain and in the wave number domain. Measuring transfer rates in steady flows is challenging, and such multidimensional measurements have not been conducted yet.

In this Letter, we perturb a rotating turbulent steady state and measure the evolution of the perturbation within a three-dimensional fluid domain. This measurement allows us to probe the energy transfer rate in the three variables mentioned above. In [40] we showed that an abrupt and short increase in the energy injection rate into existing turbulence (an injection pulse) generates wave packets of intense turbulence that propagate for long times. In the current study, we demonstrate for the first time that the spectral components of these wave packets obey the dispersion relation of inertial waves. We observe two distinct processes of energy transfer: The first, which has not been measured before, is a rapid, nonlocal process. It transfers energy from 3D, high frequency waves to low frequency quasi-2D modes. The second, slower energy transfer, is the inverse energy cascade from short to long-wave modes in the quasi-geostrophic manifold. In spite of its similarity with inverse cascade in 2D turbulence, we observe that this process too, is mediated by inertial waves propagating with a small, but nonzero z component of their wave vector.

Experimental setup.—The experimental setup is detailed in the Supplemental Material [25]. It is composed of a rotating plexiglass cylinder of 80 cm diam and 90 cm height, placed on a rotating table ($\mathbf{\Omega} = -\Omega_z \hat{\mathbf{z}}$, with a maximum rotation rate of 12.6 rad/s).

The tank is filled with water and covered with a transparent flat lid. Energy is injected at the bottom of the tank by circulating the water through an array of outlets and inlets. The energy injection is concentrated at a central wavelength $2\pi/k_{inj}$, which is a decreasing function of Ω (see Ref. [40]) down to ∼5 cm at high rotation rates.

Using a vertically scanning horizontal laser sheet, we measure the horizontal (x-y plain) velocity field, $\mathbf{u}_\perp(x, y, z, t)$, inside a $\sim 21 \times 21 \times 24$ cm^3 volume in the interior of the tank. Spatial resolution is 0.22 cm horizontally and 0.7 cm vertically, at a rate of 21.4 Hz. In each experiment, the system is brought to steady state by running it for ∼300 s with an angular speed $9.5 < \Omega < 12.5$ rad/s and a constant energy injection rate, obtaining a turbulent flow with $0.006 < \mathrm{Ro} < 0.02$ and $1500 < \mathrm{Re} < 2100$.

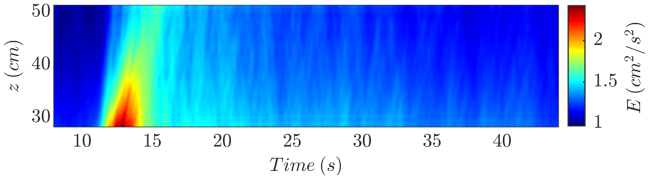

FIG. 1. Horizontally averaged energy density $E(z, t)$ for an ensemble average of 6 experiments with $\Omega = 4\pi$ rad/s. Pulse injection occurs at $t = 10.5$ s.

We then increase the pumping rate for a duration of 1.5 s, chosen as the time interval ($10.5 < t < 12$ s), after which the injection strength returns to its previous constant value. We continually measure the velocity field until $t = 60$ s. The total energy of the pulse is less than 10% of the tank's total energy. Indeed, watching a video of the energy density field [25,41], it is difficult to identify the moment of pulse injection. Each experiment is repeated 6 times, and the measurements are averaged over the repetitions.

The short increase in energy-injection generates a pulse of fluid flow with an enhanced energy density at the bottom of the tank. The pulse propagates upwards on the background of the steady-state turbulent flow (Fig. 1). During its propagation, the pulse gradually broadens and decays, exciting the entire measurement volume. The flow returns to its steady state after approximately 30 s.

We now analyze the spectral properties of the pulse as it evolves in time. To confirm that the excess energy in the pulse is composed of inertial waves, we calculated the spectral energy distribution by applying a spatiotemporal Fourier transform to the velocity field. By subtracting the steady state energy density spectrum, we were able to project the excess energy onto the frequency-polar angle plane defined by the dispersion relation Eq. (1). Our results demonstrate that the excess energy is concentrated around the dispersion relation, providing strong evidence that these waves are indeed inertial waves (see supplemental video and Supplemental Material [25,42]).

Frequency component analysis.—We now calculate the frequency-filtered velocity field $\mathbf{u}_\perp(t, \mathbf{r}; \omega)$, applying a Gaussian band-pass filter of width $\sim 0.1\Omega$ centered at ω to the measured velocity field through.

The kinetic energy density of the filtered field is $|\mathbf{u}_\perp(t, \mathbf{r}; \omega)|^2$ and we average it laterally in order to obtain $E_f(t, z; \omega)$—the energy contained in a given frequency at a given height and time. It is plotted as a function of z and t for three different values of ω in Figs. 2(a)–2(c). The high-frequency components [panels (a),(b)] propagate vertically with a finite speed that agrees with the vertical group

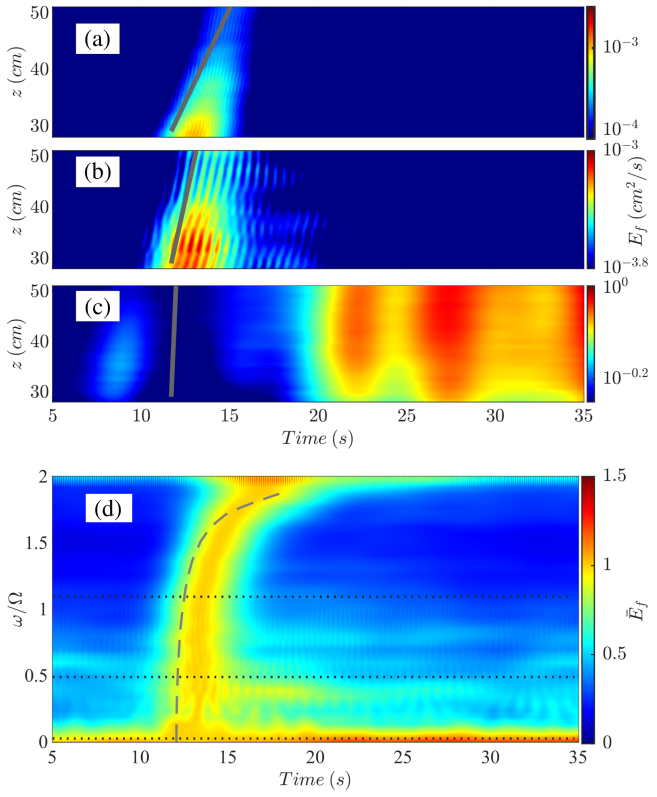

FIG. 2. Time evolution of frequency-filtered energy density. (a)–(c) Horizontally averaged energy density E_f as a function of time and vertical position z, for $\omega = 1.5\Omega(a)$, $0.6\Omega(b)$, and $0.1\Omega(c)$. Gray lines represent to the vertical group velocity of an inertial wave packet with the respective central frequency. The data was collected for experiments with $\Omega = 3.5\pi$ rad/ sec Re $\approx$ 2100 and Ro ≈ 0.006. (d) Spectrogram of fully spatially averaged energy density $\bar{E}_f$ as a function of time and ω. The energy of each frequency is normalized to 1 at the peak of the pulse. Gray dashed curve marks the theoretical arrival time of an inertial wave packet with frequency ω to the lowest measured plane.

velocity Eq. (2) for the given frequency, ω and the injection wave number $\sim$1.28 rad/cm, marked by the slopes of the gray lines in Fig. 2. These modes lose their energy within a few seconds. Contrarily, the slow, quasigeostrophic mode [panel (c)] does not propagate as a sharp front and its energy increases concurrently with the decay of the high-frequency modes. This suggests a nonlinear process of energy transfer in the frequency domain.

In order to gain insight to this process, we plot a spectrogram of the energy in the time domain,$\bar{E}_f(t;\omega)$ [Fig. 2(d)]. It is obtained via averaging $E_f(t,z;\omega)$ along z (full spatial average) together with normalization [25].

The wave packet propagation is revealed by the arrival time of the energy pulse at the lowest measured plane 28 cm above the injection plane. This dependence on ω is consistent with the predicted arrival time marked by the dashed gray line [derived from Eq. (2)]. This is an additional confirmation for the existence of the linear process of wave propagation, as observed above for the two frequencies studied in Figs. 2(a) and 2(b), marked by the upper horizontal dotted lines on the spectrogram. Another key observation is that energy is transferred from the high-frequency *directly* to the low-frequency components. The rapid decay of the energy pulse, which is clearly evident for all frequency components higher than 0.1Ω occurs concurrently with the increase in the energy of the quasigeostrophic, low-frequency modes. There is no indication for a cascade, or a gradual transfer in the frequency (orientation) domain. The rapid decay of the high frequency modes occurs within a timescale of $\tau \approx 5$ s. Notably, this timescale is consistent with indirect estimation of the dominant nonlinear time obtained by Yarom *et al.* [37] for strongly driven steady state flows. There, τ was deduced from the width of the energy spectrum. Performing similar analysis for our steady flows yields $\tau \approx 4$ s.

Since the high-frequency part of the flow is dominated by inertial waves, while the low-frequency flow is quasigeostrophic, we conclude that the energy injected by the pulse is spatially distributed by linear wave propagation. This is followed by a rapid, direct transfer of energy from modes with significant vertical wave vector components to quasi-geostrophic modes. We conjecture that this rapid process works analogously in the steady flow, forming the mechanism by which energy is fed from inertial waves and accumulates in the quasigeostrophic flow.

Spatial spectral analysis.—Next, we focus on the evolution of the energy density in wave number. For this purpose we calculate the horizontal Fourier transform of the energy density $E(z,k_{2d},t)$, and its vertical average $\bar{E}(k_{2d},t)$. Axial symmetry implies that the mean energy density depends only on the magnitude of the (horizontal) wave vector $\mathbf{k}_{2d}$. The excess energy density due to the pulse ΔE and $\Delta\bar{E}$ is obtained from E and $\bar{E}$ (respectively) by subtracting the mean steady-state energy density.

Experimental measurements of $\Delta\bar{E}$ are presented in Fig. 3(a) as a function of t and k_{2d}, with the inset showing $\Delta\bar{E}$ as a function of k_{2d} for three different times. Notably, the excess energy distribution in the quasigeostrophic manifold gradually shifts to smaller wave numbers (while the total excess energy decreases as the pulse is dissipating). The observations are consistent with a local transfer of energy from short to long-wave modes.

We quantitatively verify this scenario by following the time evolution of $k^{\star}_{2d}(t)$, the wave number of the maximum of the averaged excess energy density [Fig. 3(b)]. The linear growth of $|k^{\star}_{2d}(t)|^{-2/3}$ is consistent with the filling by a constant energy flux of a $k_{2d}^{-5/3}$ spectrum, that characterizes 2D turbulence [43–46], and was also observed in the energy spectrum of the geostrophic component of rotating turbulence [26].

These observations seem to indicate that the physics of the geostrophic component of rotating turbulence is analogous to that of 2D turbulence. However, our measurement

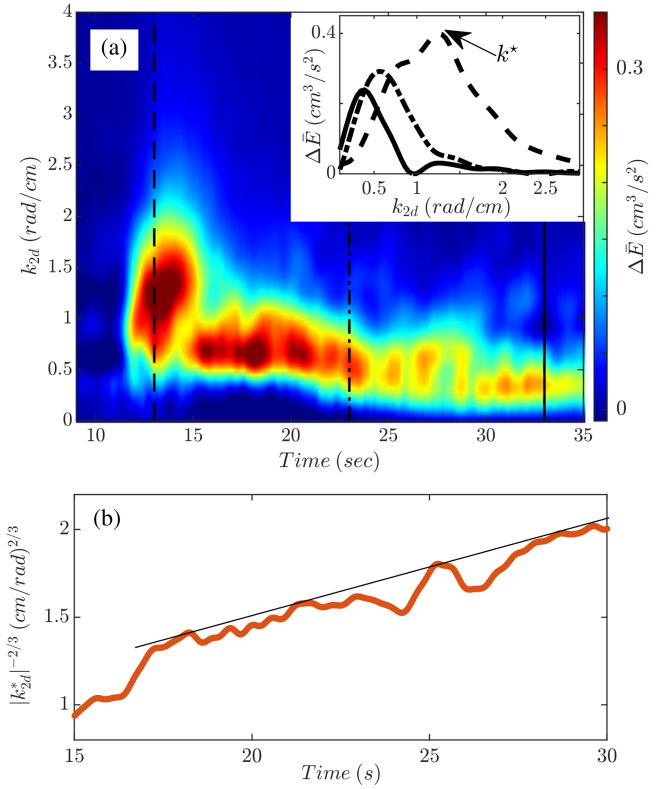

FIG. 3. (a) Vertically averaged excess energy density spectrum $\Delta\bar{E}$, as a function of time and horizontal wave number k_{2d}. Inset: $\Delta\bar{E}$ as a function of k_{2d} for $t = 13$ (dashed line), 23 (dot-dashed line), and 33 s (solid line) (marked on the main figure). The maximum of the instantaneous $\Delta\bar{E}$, $k^\star_{2d}(t)$, is indicated for $t = 13$ s. The gradual shift of the excess energy to lower wave numbers is a manifestation of the inverse energy cascade. (b) $|k^\star_{2d}|^{-2/3}$ as a function of time. The agreement with linear growth beyond $t = 17$ s indicates $k^\star_{2d} \sim t^{-2/3}$. The dataset is the same as in panel (a).

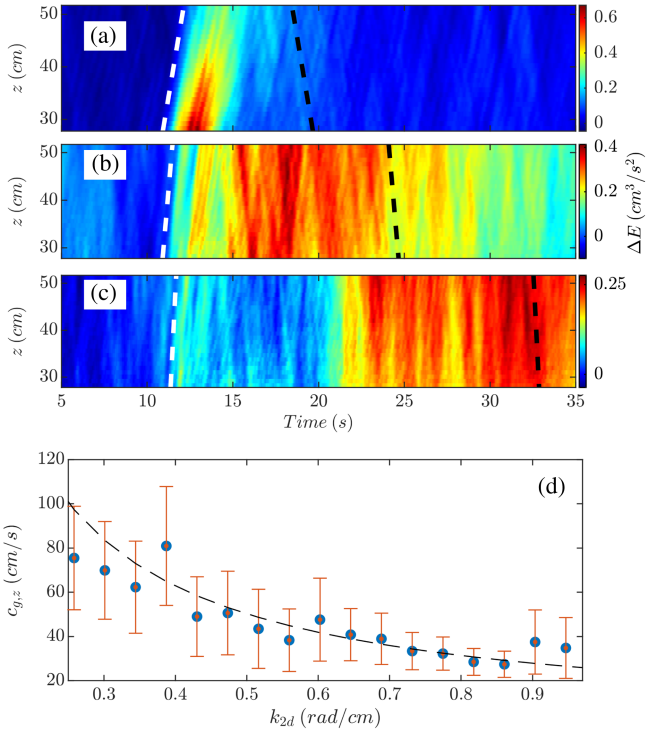

FIG. 4. (a)–(c) Excess energy density at fixed wave number, $\Delta E(z, k_{2d}, t)$, as a function of vertical position z and time (showcasing the same data as Fig. 3, with vertical resolution). The fixed wave numbers in each subplot are $k_{2d} = 2.28$(a), 0.6(b), and 0.34(c) rad/cm. Slopes of the dashed lines indicate $C_{g,z}$ for the relevant wave number and $\theta = \pi/2$ for waves that propagate upwards (white) and downwards (black). As time increases, energy cascades from large to small wave numbers while propagating vertically up and down. (d) Estimation of the energy propagation speed for each wave number k_{2d} (symbols), compared with $C_{g,z}(k_{2d})$ from Eq. (2) (dashed curve).

of the z-dependent energy density, reveals a weak but significant vertical variation in $\Delta E(z, k_{2d}, t)$. Indeed, the plots of $\Delta E(z, k_{2d}, t)$ as a function of z, t for three fixed values of k_{2d} [Figs. 4(a)–4(c)] exhibit *diagonal* rather than vertical correlations, indicating that information travels vertically at a finite speed, while transferring energy to broader horizontal scales. Moreover, the propagation speed is given by the vertical group velocity component (2), evaluated at k_{2d}, with $\theta = \pi/2$. These waves propagate upwards (white lines) as well as downwards (black lines). Evidence for inertial wave carrying the *excess* energy persists during the entire inverse energy cascade from the large wave numbers in Fig. 4(a), through intermediate (b) to small wave numbers (c). These observations provide strong evidence that the energy that was shown to inversely cascade in Fig. 3 consists of (nearly horizontal) inertial waves.

Using a Hough transform of the measured $\Delta E(z, k_{2d}, t)$ for each k_{2d} [25] we show that the vertical propagation velocity is consistent with the k dependence of $C_{g,z}$ [Fig. 4(d)].

Discussion.—We used an injection pulse—a perturbation, localized in time and space, of the energy injection, in order to monitor energy transfer rates in developed rotating turbulence. Assuming that the kinetics that govern the pulse are similar to those of the statistically stationary steady state flow, these measurements facilitate experimental observation of three energy transfer processes: spatial homogenization, transfer of energy from high frequency 3D modes to low-frequency quasigeostrophic modes, and the inverse cascade of energy within the quasigeostrophic manifold, which carries the majority of energy in steady state.

The spatial homogenization of energy is achieved by inertial wave propagation, which is the fastest process in the system, and is well described by linear inertial wave theory, even though the waves are strong and propagate on the background of a turbulent flow.

The injected energy is dominated by inertial waves with 3D wave vectors. However, the resulting 3D flow field is a

short-lived transient, whose energy is siphoned away towards the geostrophic flow. The depletion of the 3D modes occurs on a dynamical timescale determined by interaction of inertial waves with the geostrophic flow [32,37,40].

Energy flows directly from wave vectors with arbitrary polar angles to quasigeostrophic wave vectors, bypassing intermediate ones (Fig. 2). This strongly indicates that the energy transfer in the frequency (orientation) domain is not mediated by intermediate interactions or a cascade.

Once the pulse energy has reached the quasigeostrophic manifold, it gradually flows to smaller wave numbers in a manner consistent with an inverse cascade of energy. This observations seems consistent with dynamics analogous to the Kraichnan cascade of 2D turbulence [43,45]. However, an analysis of the vertically resolved horizontal Fourier transform of the flow shows conclusively that the inverse cascade in Fourier space takes place in parallel with spatial propagation consistent with the linear dynamics of inertial waves. This shows that inertial waves participate in all known energy transfer processes, making the analogy between the rotating turbulence inverse cascade the Kraichnan cascade tenuous.

Some of our results are directly related to theoretical models of rotating turbulence. In this strongly driven regime we find two nonlinear processes with different timescales: rapid flattening and a slow inverse cascade, such observations are qualitatively consistent with theoretical predictions [23,33,36]. However, our data exclude energy cascade in the frequency domain (or orientation). This unambiguous result contradicts assumptions incorporated in some of theoretical models [4,31]. In addition, to the best of our knowledge, the mediation of the inverse energy cascade by propagating waves was not discussed in theoretical modeling.

We are, therefore, left with several open questions that call for further work: Do the observed propagating modes play a central role in the inverse energy cascade, or are they 3D "artifacts" of the inherently 2D process? Is the infinite (in z) medium case a singular limit of the problem? It is possible that the separation to 2D and 3D flow components, as well as the focusing on the exact 2D manifold, are not well determined in finite systems. We hope that further theoretical and experimental works will shed light on these important issues.

This research was supported by the Israel Science Foundation Grants No. 2437/20 and No. 2403/20. A. S. gratefully acknowledges the support of the Clore Israel Foundation Scholars Program, the Israeli Council for Higher Education, and the Milner Foundation.

[1] J. Pedlosky *et al.*, *Geophysical Fluid Dynamics* (Springer, New York, 1987), Vol. 710.
[2] P. A. Davidson, *Turbulence in Rotating, Stratified and Electrically Conducting Fluids* (Cambridge University Press, Cambridge, England, 2013).
[3] P. A. Davidson, *Turbulence: An Introduction for Scientists and Engineers* (Oxford University Press, New York, 2015).
[4] A. Alexakis and L. Biferale, Cascades and transitions in turbulent flows, Phys. Rep. **767**, 1 (2018).
[5] J. F. Scott, Wave turbulence in a rotating channel, J. Fluid Mech. **741**, 316 (2014).
[6] A. van Kan and A. Alexakis, Critical transition in fast-rotating turbulence within highly elongated domains, J. Fluid Mech. **899**, A33 (2020).
[7] H. P. Greenspan *et al.*, *The Theory of Rotating Fluids* (Cambridge University Press, Cambridge, England, 1968).
[8] The dispersion relation for inertial waves has a symmetry with respect to the transformation $\omega \to -\omega$ and $k_z \to -k_z$, so it is redundant to calculate the distribution of negative frequencies in time. we will assume that k_z can be negative and ω is positive.
[9] G. Bordes, F. Moisy, T. Dauxois, and P.-P. Cortet, Experimental evidence of a triadic resonance of plane inertial waves in a rotating fluid, Phys. Fluids **24**, 014105 (2012).
[10] M. Brunet, B. Gallet, and P.-P. Cortet, Shortcut to geostrophy in wave-driven rotating turbulence: The quartetic instability, Phys. Rev. Lett. **124**, 124501 (2020).
[11] E. Yarom and E. Sharon, Experimental observation of steady inertial wave turbulence in deep rotating flows, Nat. Phys. **10**, 510 (2014).
[12] A. Campagne, B. Gallet, F. Moisy, and P.-P. Cortet, Disentangling inertial waves from eddy turbulence in a forced rotating-turbulence experiment, Phys. Rev. E **91**, 043016 (2015).
[13] M. Duran-Matute, J.-B. Flór, F. S. Godeferd, and C. Jause-Labert, Turbulence and columnar vortex formation through inertial-wave focusing, Phys. Rev. E **87**, 041001(R) (2013).
[14] C. Cambon, N. N. Mansour, and F. S. Godeferd, Energy transfer in rotating turbulence, J. Fluid Mech. **337**, 303 (1997).
[15] F. S. Godeferd and F. Moisy, Structure and dynamics of rotating turbulence: A review of recent experimental and numerical results, Appl. Mech. Rev. **67**, 030802 (2015).
[16] I. Kolvin, K. Cohen, Y. Vardi, and E. Sharon, Energy transfer by inertial waves during the buildup of turbulence in a rotating system, Phys. Rev. Lett. **102**, 014503 (2009).
[17] P. Davidson, P. Staplehurst, and S. Dalziel, On the evolution of eddies in a rapidly rotating system, J. Fluid Mech. **557**, 135 (2006).
[18] P. Staplehurst, P. Davidson, and S. Dalziel, Structure formation in homogeneous freely decaying rotating turbulence, J. Fluid Mech. **598**, 81 (2008).
[19] G. P. Bewley, D. P. Lathrop, L. R. Maas, and K. Sreenivasan, Inertial waves in rotating grid turbulence, Phys. Fluids **19**, 071701 (2007).
[20] C. Morize, F. Moisy, and M. Rabaud, Decaying grid-generated turbulence in a rotating tank, Phys. Fluids **17**, 095105 (2005).
[21] S. Galtier, Weak inertial-wave turbulence theory, Phys. Rev. E **68**, 015301(R) (2003).
[22] S. Nazarenko, *Wave Turbulence* (Springer Science & Business Media, New York, 2011), Vol. 825.

[23] L. M. Smith and F. Waleffe, Transfer of energy to two-dimensional large scales in forced, rotating three-dimensional turbulence, Phys. Fluids **11**, 1608 (1999).
[24] E. Monsalve, M. Brunet, B. Gallet, and P.-P. Cortet, Quantitative experimental observation of weak inertial-wave turbulence, Phys. Rev. Lett. **125**, 254502 (2020).
[25] See Supplemental Material at http://link.aps.org/supplemental/10.1103/PhysRevLett.132.224001 for detailed description of the experimental system, procedures and definitions used in the article and in the supplemental videos; additional measurements at different parameters and for weakly driven results.
[26] E. Yarom, Y. Vardi, and E. Sharon, Experimental quantification of inverse energy cascade in deep rotating turbulence, Phys. Fluids **25**, 085105 (2013).
[27] M. Buzzicotti, P. Clark Di Leoni, and L. Biferale, On the inverse energy transfer in rotating turbulence, Eur. Phys. J. E **41**, 1 (2018).
[28] A. Sen, P. D. Mininni, D. Rosenberg, and A. Pouquet, Anisotropy and nonuniversality in scaling laws of the large-scale energy spectrum in rotating turbulence, Phys. Rev. E **86**, 036319 (2012).
[29] C. N. Baroud, B. B. Plapp, H. L. Swinney, and Z.-S. She, Scaling in three-dimensional and quasi-two-dimensional rotating turbulent flows, Phys. Fluids **15**, 2091 (2003).
[30] C. Lamriben, P.-P. Cortet, and F. Moisy, Direct measurements of anisotropic energy transfers in a rotating turbulence experiment, Phys. Rev. Lett. **107**, 024503 (2011).
[31] A. Campagne, B. Gallet, F. Moisy, and P.-P. Cortet, Direct and inverse energy cascades in a forced rotating turbulence experiment, Phys. Fluids **26**, 125112 (2014).
[32] P. C. di Leoni and P. D. Mininni, Quantifying resonant and near-resonant interactions in rotating turbulence, J. Fluid Mech. **809**, 821 (2016).
[33] T. Le Reun, B. Gallet, B. Favier, and M. Le Bars, Near-resonant instability of geostrophic modes: Beyond Greenspan's theorem, J. Fluid Mech. **900**, R2 (2020).
[34] F. Bellet, F. Godeferd, J. Scott, and C. Cambon, Wave turbulence in rapidly rotating flows, J. Fluid Mech. **562**, 83 (2006).
[35] B. Gallet, Exact two-dimensionalization of rapidly rotating large-reynolds-number flows, J. Fluid Mech. **783**, 412 (2015).
[36] S. V. Nazarenko and A. A. Schekochihin, Critical balance in magnetohydrodynamic, rotating and stratified turbulence: Towards a universal scaling conjecture, J. Fluid Mech. **677**, 134 (2011).
[37] E. Yarom, A. Salhov, and E. Sharon, Experimental quantification of nonlinear time scales in inertial wave rotating turbulence, Phys. Rev. Fluids **2**, 122601(R) (2017).
[38] T. Le Reun, B. Favier, A. J. Barker, and M. Le Bars, Inertial wave turbulence driven by elliptical instability, Phys. Rev. Lett. **119**, 034502 (2017).
[39] P. Clark Di Leoni, P. J. Cobelli, P. D. Mininni, P. Dmitruk, and W. Matthaeus, Quantification of the strength of inertial waves in a rotating turbulent flow, Phys. Fluids **26**, 035106 (2014).
[40] A. Salhov, E. Yarom, and E. Sharon, Measurements of inertial wave packets propagating within steady rotating turbulence, Europhys. Lett. **125**, 24003 (2019).
[41] Online video: Energy density in time, shown on three planes of the volume and on a vertical plane (2023).
[42] Online video: Excess energy spectrum, on the $\omega - \theta$ plane (2023).
[43] R. H. Kraichnan, Inertial ranges in two-dimensional turbulence, Phys. Fluids **10**, 1417 (1967).
[44] U. Frisch and P.-L. Sulem, Numerical simulation of the inverse cascade in two-dimensional turbulence, Phys. Fluids **27**, 1921 (1984).
[45] P. Tabeling, Two-dimensional turbulence: A physicist approach, Phys. Rep. **362**, 1 (2002).
[46] J. Paret and P. Tabeling, Experimental observation of the two-dimensional inverse energy cascade, Phys. Rev. Lett. **79**, 4162 (1997).